Journal of Molecular Biology and Molecular Imaging

Open Access

Austin Publishing Group

Research Article

Molecular Imaging of VEGF Expression in Multiple Myeloma and Non-Hodgkin Lymphoma

Camacho X[1]*, Perroni C[1], Carneiro CG[2], Junqueira MS[2], Machado CL[2], Faria D[2], García MF[1], Fernández M[1], Buchpiguel CA[2], Cerecetto H[1], Chammas R[3], Riva E[4], Cabral P[1] and Gambini JP[5]

[1]Departamento de Radiofarmacia, Centro de Investigaciones Nucleares, Facultad de Ciencias, Universidad de la República, Montevideo, Uruguay

[2]Nuclear Medicine Medical Investigation Laboratory LIM43, Hospital das Clínicas da Faculdade de Medicina da Universidade de Sao Paulo-HCFMUSP, Sao Paulo, Brazil

[3]Laboratório de Oncologia Experimental, Faculdade de Medicina, Universidade de São Paulo, Av. Dr. Arnaldo Nº 455- Cerqueira César - CEP: 01246903, São Paulo, Brazil

[4]Clínica Hematológica, Hospital de Clínicas, Facultad de Medicina, Universidad de la República, Montevideo, Uruguay

[5]Centro de Medicina Nuclear e Imagenología Molecular, Hospital de Clínicas, Facultad de Medicina, Universidad de la República, Montevideo, Uruguay

***Corresponding author:** Camacho X, Departamento de Radiofarmacia, Centro de Investigaciones Nucleares, Facultad de Ciencias, Universidad de la República, Montevideo, Uruguay. Mataojo 2055, P.O. 11400, Montevideo, Uruguay

Received: January 25, 2022; **Accepted:** February 21, 2022; **Published:** February 28, 2022

Abstract

Angiogenesis is a crucial process in the growth, development, and metastasis of many tumor types, including Non-Hodgkin's lymphoma (NHL) and Multiple Myeloma (MM). Vascular endothelial growth factor (VEGF) overexpression is known to be associated with poor prognosis in both pathologies, representing a rational target for anti-angiogenic therapy in NHL and MM. The monoclonal antibody Bevacizumab binds to VEGF with high affinity and blocks its action. We aim to evaluate Bevacizumab as a potential radioactive and fluorescence agent for imaging VEGF expression in MM and NHL.

Flow cytometry analysis revealed VEGF expression in MM and NHL cell lines is mainly intracellularly. Biodistribution and Single-photon emission computed tomography/computed tomography (SPECT/CT) studies of ^{99m}Tc-HYNIC-Bevacizumab showed a slow blood clearance and supradiaphragmatic, head, axial and appendicular skeleton can be evaluated without much interference. Tumor-to-muscle ratio increased with time and is similar to the ones reported with other ^{99m}Tc-radiolabeled antibodies. Cy7-Bevacizumab fluorescent imaging allowed MM and NHL tumor visualization with greater spatial resolution than SPECT/CT.

We successfully synthesized ^{99m}Tc and Cy7-labeled anti-VEGF mAb (Bevacizumab) to be used to target VEGF expression *in vivo* in MM and LNH. Our encouraging results, although working with ^{99m}Tc, highlight the importance of radioinmuno-oncology as a potential tool to fight these diseases. Optical imaging of these tracers would enhance tumor sampling and guide surgical removal.

Keywords: Bevacizumab; Molecular Imaging; VEGF; Multiple Myeloma; Non-Hodgkin Lymphoma; ^{99m}Technetium- or Cy7-lableled Bevacizumab

Abbreviations

NHL: Non-Hodgkin's Lymphoma; MM: Multiple Myeloma; VEGF: Vascular Endothelial Growth Factor; SPECT/CT: Single-Photon Emission Computed Tomography/Computed Tomography; VEGFRs: Vascular Endothelial Growth Factor Receptors; RTKs: Recetor Tyrosine Kinases; NIR: Near Infrared; NHS-HYNIC-Tfa: Trifluoroacetyl Hydrazino-Protected Form of the Succinimidyl Ester of HYNIC; BCA: Bifunctional Chelating Agent; ATCC: American Type Culture Collection; PBS: Phosphate Buffered Saline; PFA: Paraformaldehyde; BSA: Bovine Serum Albumin; FITC: Fluorescein Isothiocyanate; RT: Room Temperature; SEC: Size-Size Exclusion Chromatography; MALDI TOF/TOF: Matrix-Assisted Laser Desorption/Ionization/Time-of-Flight; ITLC: Instant Thin Layer Chromatography; HPLC: High Performance Liquid Chromatography; % ID: Percentage of the Injected Dose; % ID/g: Percentage of the Injected Dose per Gram of Tissue; Cy7-NHS ester: Cy7-Monofunctional N-Hydroxysuccinimide ester; DMSO: Dimetyilsufoxide; $MWB_{evacizumab}$: Molecular Weight of Bevacizumab; ε_{cy7}: Extinction Coefficient of Cy7 at Abs_{747}

Introduction

NHL and MM are lymphoproliferative diseases. VEGF overexpression occurs in many human tumors types, including lymphoproliferative disorders such as NHL and MM, which have been associated with poor prognosis [1-9].

VEGF family includes a large number of factors: VEGF-A, VEGF-B, VEGF-C, VEGF-D, and placental growth factor. Each one of them has their own receptor specificities and biological properties. VEGF family most known factor is VEGF-A which has different variants (VEGF121, VEGF145, VEGF148, VEGF165, VEGF183, VEGF189, and VEGF206), having each one diferente function and receptor specificity [10]. One of VEGF most important properties is to promote vascular endothelial cells growth and can prevent their apoptosis. It can also induce endothelial fenestration, modulating vascular permeability [11]. It has been established that many cytokines and grow factors could be responsible of VEGF mRNA expression upregulation or induce VEGF release [12]. Also VEGF has been shown to influence immune and cancer cells, although the exact mechanisms behind them are yet to be discovered [13].

Once VEGF role in angiogenesis was discovered, many inhibitors were developed in order to treat cancer [14-31]. In this way we can find anti-VEGF or anti-VEGFR monoclonal antibodies, small molecular inhibitors of recetor tyrosine kinases (RTKs) of VEGFRs [16,21,24,27,32-36]. One of the most popular anti VEGF antibodies is Bevacizumab (rhuMAb-VEGF, Avastin®, Genentech, USA) [37,38].

Citation: Camacho X, Perroni C, Carneiro CG, Junqueira MS, Machado CL, Faria D, et al. Molecular Imaging of VEGF Expression in Multiple Myeloma and Non-Hodgkin Lymphoma. J Mol Biol & Mol Imaging. 2022; 7(1): 1033.

Some of these antiangiogenic molecules have been radiolabeled in order to produce a diagnostic and/or therapeutic agent [39-87], having the potential to detect emerging tumors, monitor the response to treatment and predict treatment outcomes as well as refer patients that could benefit from anti angiogenic therapy. These molecules can also be labeled with a fluorescent dye in order to provide high-resolution, real-time imaging of VEGF tumor expression [72,73,83], allowing to guide surgeries. NIR fluorophores have been increasingly used in this setting due to their reasonable penetration with almost no tissue autofluorescence [88,89]. Taking these facts into consideration the aim of this work was to develop new potential radioactive and fluorescent agents for imaging VEGF expression in NHL and MM. To this end, we labeled Bevacizumab with Cy7 and with ^{99m}Tc *via* NHS-HYNIC-Tfa as BCA.

Materials and Methods

Cell culture

Human MM and B-cell NHL cell lines (MM1S and Toledo) were obtained from ATCC and from Banco de Células do Rio de Janeiro, respectively. All cell lines were grown in RPMI-1640, pH 7.4, supplemented with 10% fetal bovine serum, 100U/mL penicillin and 100µg/mL streptomycin. All cells were maintained at 37°C in a 5% CO_2 incubator.

Flow cytometry analyses

Bevacizumab (Avastin™ anti-VEGF monoclonal antibody) produced by Genetech, Inc., was provided by Roche Laboratories, Uruguay.

Surface staining: After culture disaggregation the cells were washed 3 times in PBS (5min, 600g) and fixed in 2% cold and freshly prepared PFA in PBS. Samples were then incubated at 4°C for 15min. Following cross-linking fixation, cells were blocked for 1h at 4°C with PBS-3% BSA, and then incubated with 2µg of Bevacizumab-FITC (2mg/mL) in PBS-1% BSA. After 2h of incubation in the dark at 37°C, the cells were washed 3 times in PBS (5min, 600g). Data were acquired in a FACSCALIBUR® flow cytometer (BD Biosciences, San Jose, CA, USA) and analyzed using FlowJo software (Becton Dickinson & Company, Franklin Lakes, NJ, USA) [42].

Intracellular staining: After culture disaggregation in PBS, fixed in 2% PFA and washed, cells were permeabilized with 200µl of 0.2% (v/v) Tween-20 in PSA for 30min at 4°C. Then, cells were washed 3 times in PBS-1% BSA (5min, 600g) to remove 0.2% (v/v) Tween-20 from the medium, blocked for 1h at 4°C with PBS-BSA 3% and incubated with 2µg of Bevacizumab-FITC for1 h at 37°C in the dark. Then the cells were washed 3 times in PBS (5min, 600g). Data were acquired and analyzed as previously described in 2.2.1 section.

Controls for surface and intracellular staining included cells alone, isotype-FITC control (2µg for each batch) to determine autofluorescence levels, or unspecific reactions [42].

Linker Formation between HYNIC and Bevacizumab, radiolabeling with ^{99m}-Technetium and quality controls

NHS-HYNIC-Tfa was synthesized and conjugated to Bevacizumab as previously described by our group [39-43,54]. Briefly, 0.067µmol of Bevacizumab was mixed at RT for 30min with 0.33µmol of NHS-HYNIC-Tfa. The conjugate was purified by SEC and used MALDI TOF/TOF lineal to determine the level of conjugation.

Radiolabeling Bevacizumab with ^{99m}-Technetium and quality controls were performed as previously described by our group [39-43,54]. For this purpose, 44.6mol of Tricine, 44.3mol of $SnCl_2.2H_2O$ and 6.7nmol of antibody conjugate were mixed, and immediately a Na $^{99m}TcO_4$ solution was added. The mixture was incubated at RT for 30min and the radiochemical purity was evaluated by ITLC and HPLC [39,41]. The integrity of radiolabeled Bevacizumab was analyzed by HPLC by incubation at 37°C in 0.9% NaCl, serum and in different concentrations of L-Cysteine.

Animals and tumor induction

Healthy male BALB/c and BALB/c nude mice, 8-10-weeks-old (20-24 g), were obtained from the Animal House Facility of the Universidad de la República, Uruguay and from Animal House Facility of the Faculdade de Medicina da Universidade de São Paulo. All animals were maintained in ventilated cages in ventilated racks with sterilized food and water ad libitum, in a 12/12 h light/dark cycle.

Toledo and MM1S cells at a 0.5 x 10^7 concentration (with at least 95% of viable cells) were subcutaneously injected in male BALB/c nude mice. The animals were followed daily for at least 1 month, evaluating tumor growth.

All procedures were in accordance with ethical principles adopted by Uruguayan Animal Experimentation Ethics Committee (procedure approval number 240011-002308-14) and Brazilian College of Animal Experimentation and approved by the Ethical Committee for Animal Research of the Faculdade de Medicina da Universidade de São Paulo (procedure approval number 279/12) [42,43,54].

In vivo biodistribution studies

^{99m}Tc-HYNIC-Bevacizumab biodistribution studies were performed on healthy male BALB/c mice and Toledo and MM1S tumor-bearing BALB/c nude mice (n=5 per group per time) as previously described by our group [42,43,54]. Briefly, animals were injected *via* intravenous tail with approximately 1.8MBq/100ug of radiolabeled Bevacizumab and euthanized by anesthetic drugs (xilazin-100mg/Kg and ketamin-300mg/Kg) after 2, 6 and 24 h. Selected tissues (heart, liver, lungs, thyroid, kidneys, stomach, spleen, gastrointestinal tract and bladder) were excised, rinsed of residual blood, weighed and their radioactivity measured in an dose Calibrator Capintec CRC7, Solid Scintillation counter with 3"x3" NaI(Tl) crystal detector associated to a ORTEC multichannel analyzer. Urine, blood, tumor (site of inoculation of the MM1S cell line in the MM model and lymph nodes in LNH model) were also collected together and measure. Organ activity was expressed as % ID and as % ID/g.

Bevacizumab-Cy7 conjugation

Bevacizumab-Cy7 conjugation was performed as previously described by our group [42,43]. Briefly, a solution of 500µL of Bevacizumab (0.5mg/mL) and 500µL of 0.15M NaCl was mixed and centrifuged at 14,000g for 10min at 4°C using a Centricom-30 ultrafiltration device. The buffer was then changed to 0.1M $NaHCO_3$ (pH 8.3). One milliliter of Bevacizumab solution (0.5mg/mL) was mixed with a solution of Cy7-NHS ester diluted in DMSO. The reaction was carried out for 2h in complete darkness. To separate the free dye, the mixture was centrifuged at 14,000 xg for 10min at

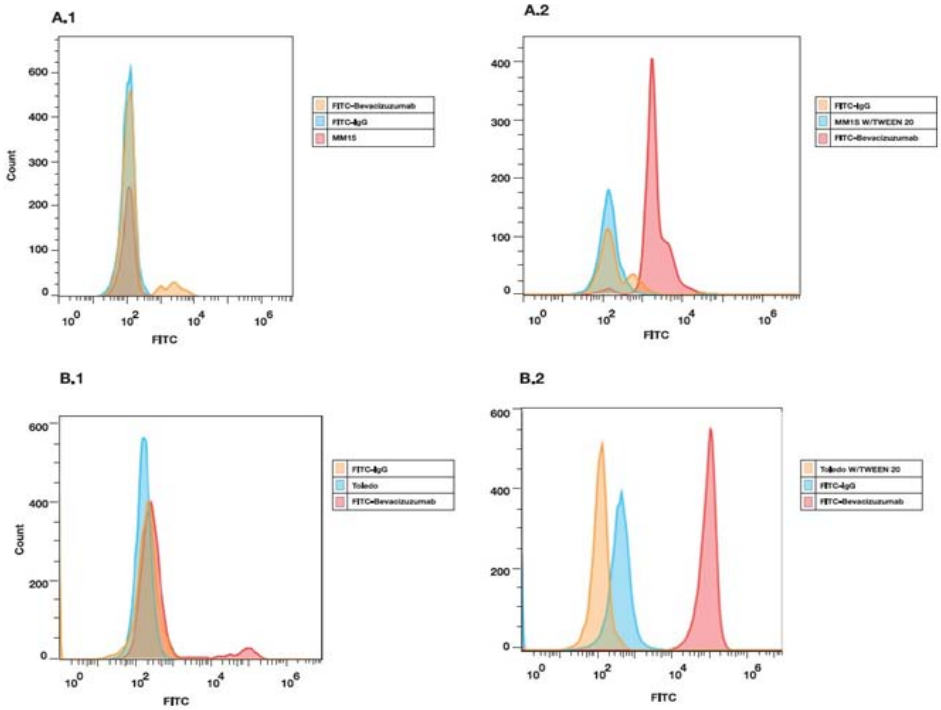

Figure 1: Flow cytometry assay. Expressions levels of VEGF in MM1S and Toledo cell lines were assessed by flow cytometry using FITC-Bevacizumab. Cell Surface (A.1 and B.1) and intracellular (A.2 and B.2) staining is shown.

4°C with a Centricom-30 ultrafiltration device and the sample was subsequently replaced with PBS.

The protein concentration in mg/mL was calculated according to the following formula: mg/mL Protein = (Abs_{280} - 0.04 x Abs_{747})/1.4

The ratio of Cy7: Bevacizumab in the final conjugate was calculated according to the following formula: ratio of Cy7/ Bevacizumab = (Abs_{747} x MWBevacizumab)/mg/mL Protein x ε_{cy7} (ε_{cy7} = 210000$cm^{-1}M^{-1}$)

Molecular imaging

SPECT/CT imaging: SPECT/CT images were performed on a μPET/SPECT/CT instrument (Triumph, Trifoil Imaging Inc.) as previously described by our group [42,43,54]. After 7 days of inoculation of MM1S and Toledo cell lines into female BALB/c nude mice, a mixture of 2-2.5% isoflurane and oxygen were used for anesthesia, followed by an intravenous tail injection of ^{99m}Tc-HYNIC-Bevacizumab (100μg, 74-111 MBq/mice). After 6 and 24 h SPECT/CT images were acquired with a five-pin hole collimator (0.8mm spatial resolution, 55 x 55 mm trans-axial field of view, 64 projections, FOV=46mm) and reconstructed with an OSEM filter (5 interactions with 8 subsets) correction in a 20% of a ^{99m}Tc-window followed by a DICOM generation by the Amira 4.1 software and the co-registration were analyzed by Amide software [55].

Fluorescent imaging: *In vivo* fluorescent imaging of MM1S and Toledo tumor-bearing mice with Cy7-Bevacizumab (100μg) was performed to assess tumor uptake up 96h p.i [42,43]. A healthy, Cy7-Bevacizumb uninjected Balb/c nude mouse was used as a control. Images were acquired with 745nm excitation and 800nm emission filters in an iVis Spectrum charge-couples device camera. Fluorescence images was quantified by total radiant efficiency quantification ((photons/s)/(μW/cm^2)) using Living Image 4.3.1 software. During fluorescence examination, all animals were anesthetized with a 1-2% of isoflurane-oxygen mixture to enable imaging studies to be performed.

Statistical analysis

Data was analyzed using one-way ANOVA followed by Bonferroni post-hoc tests using GraphPad Prism 4.0 software. Differences were considered significant when $p<0.5$ [43,54].

Results

Flow cytometry analyses

The VEGF expression levels of human MM1S and Toledo cells lines were analyzed by flow cytometry using FITC-Bevacizumab. Figure 1 shows the surface marker (A.1 and B.1) and intercellular profile (A.2 and B.2) of MM1S and Toledo cell lines. Therefore, since VEGF was mostly detected by intracellular staining, this confirms that its expression is at this level.

In vivo biodistribution studies

In vivo biodistribution studies in healthy male BALB/c, MM1S and Toledo male BALB/c nude tumor-bearing mice are showed in Figure 2-4.

Blood radioactivity levels in healthy mice were 25.44 ± 2.78 %ID/g and 11.04 ± 2.83 %ID/g at 6 and 24 h p.i., respectively. MM1S tumor-bearing BALB/c nude mice blood radioactivity levels were 15.55 ± 4.48 %ID/g and 10.43 ± 0.93 %ID/g at 6 and 24 h p.i., respectively. Toledo tumor-bearing BALB/c nude mice blood radioactivity levels were 18.74 ± 1.62 ID/g and 14.34 ± 2.64 ID/g at 6 and 24 h p.i,

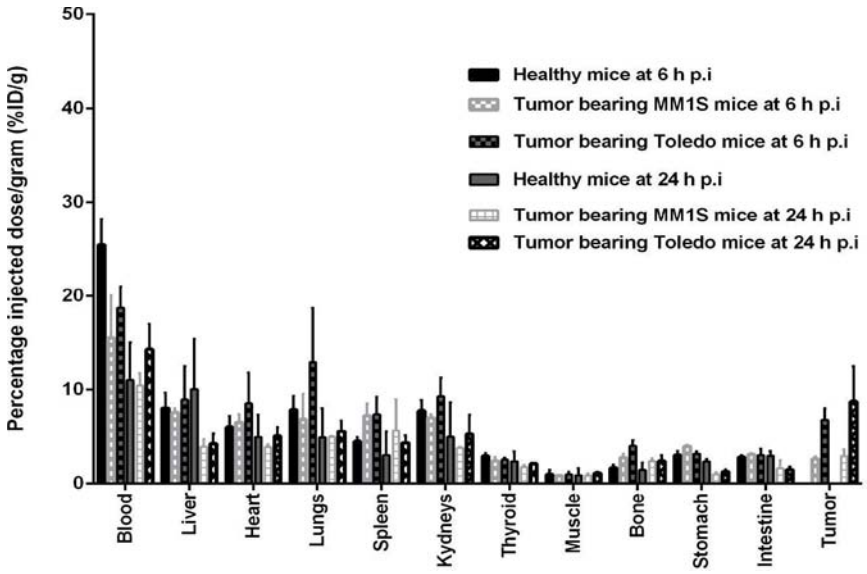

Figure 2: Healthy BALB/c and MM1S and Toledo tumor-bearing BALB/c nude mice biodistribution studies of ^{99m}Tc-HYNIC-Bevacizumab at 6 and 24 h p.i. Values are expressed as % ID per gram (or % ID/g) (mean ± SD, n=5).

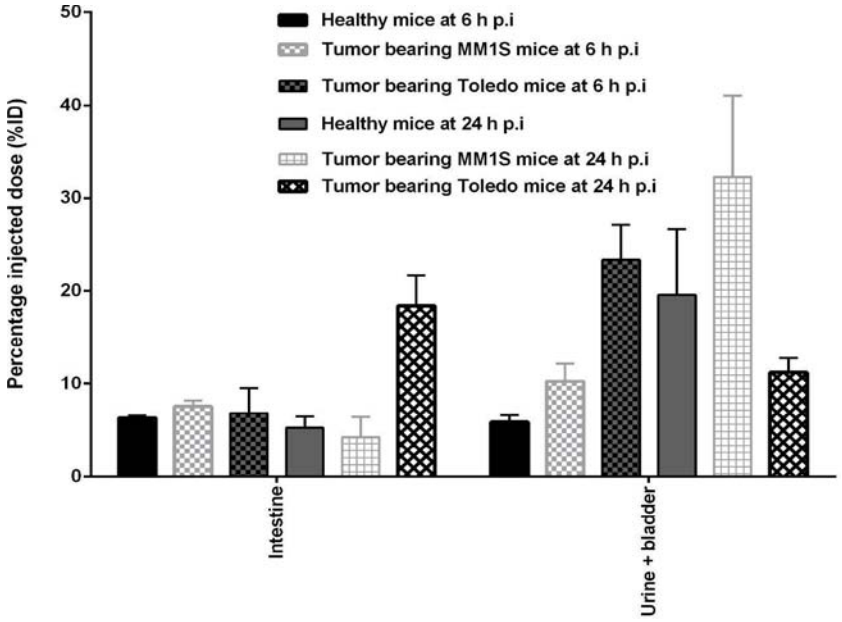

Figure 3: Healthy BALB/c and MM1S and Toledo tumor-bearing BALB/c nude mice biodistribution studies of ^{99m}Tc-HYNIC-Bevacizumab at 6 and 24 h p.i. Values are expressed as % ID (or % ID) (mean ± SD, n=5).

respectively. This shows a slow clearance of radiolabeled antibody from the blood.

Liver radioactivity levels in healthy mice were 8.50 ± 1.62 %ID/g and 10.25 ± 2.25 %ID/g at 6 and 24 h p.i, respectively. MM1S tumor-bearing BALB/c nude mice liver radioactivity levels were 7.59 ± 0.43 %ID/g and 3.93 ± 0.56 %ID/g at 6 and 24 h p.i., respectively. Toledo tumor-bearing BALB/c nude mice liver radioactivity levels were 8.96 ± 2.48 ID/g and 4.25 ± 1.07 ID/g at 6 and 24 h p.i, respectively. Also, kidney radioactivity levels in healthy mice were 7.77 ± 1.13 %ID/g and 4.98 ± 2.61 %ID/g at 6 and 24 h p.i, respectively. MM1S tumor-bearing BALB/c nude mice kidney radioactivity levels were 7.03 ± 0.35 %ID/g and 3.79 ± 0.05 %ID/g at 6 and 24 h p.i., respectively. Toledo tumor-bearing BALB/c nude mice kidney radioactivity levels were 9.31± 1.40 %ID/g and 5.23 ± 2.13 %ID/g at 6 and 24 h p.i, respectively. Liver and kidney uptake were related to radiolabeled antibody clearance. Also, gastrointestinal radioactivity levels in healthy and MM1S and Toledo tumor-bearing BALB/C nude was present related to hepatic clearance of the antibody. At 24h p.i. (19.59 ± 5.00 %ID, 32.01 ± 5.96 %ID and 11.25 ± 1.50 %ID) of ^{99m}Tc-HYNIC-Bevacizumab had been excreted in the urine. Less than 4 %ID/g was present in muscle, bone, thyroid and stomach at all analyzed time points.

MM1S tumor-bearing BALB/c nude mice lungs and intestine

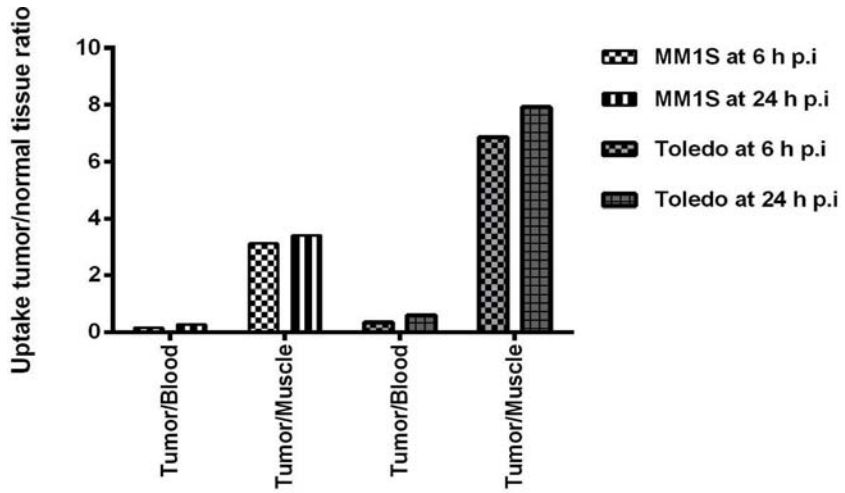

Figure 4: Tumor-to-blood and tumor-to-muscle ratios of ^{99m}Tc-HYNIC-Bevacizumab in MM1S and Toledo tumor-bearing BALB/c nude mice at 6 and 24 h p.i.

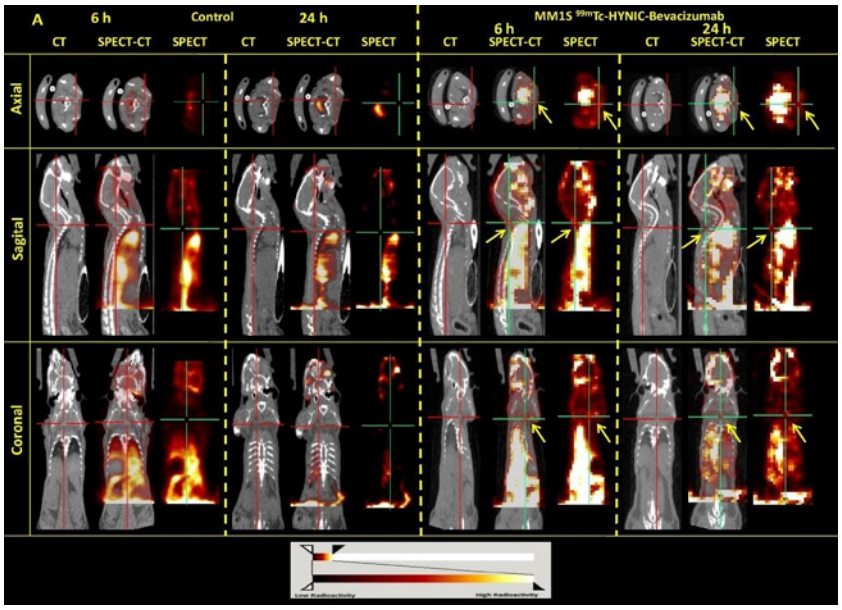

Figure 5: SPECT/CT axial, sagital and coronal images at 6 and 24 h post-injection of ^{99m}Tc-HYNIC-Bevacizumab on healthy (A) and MM1S tumor-bearing BALB/c nude mice (B). BALB/c nude mice SPECT/CT image shows non homogeneous heart, spleen, liver, kidney, bladder and gastrointestinal uptake and MM1S tumor-bearing BALB/c nude mice SPECT/CT shows a remarkable uptake of the radiolabeled Bevacizumab in the site of cell inoculation (tumor uptake, yellow arrows).

radioactivity levels were 6.87 ± 2.66 %ID/g and 3.10± 0.15 %ID/g, 4.97 ± 0.05 and 1.61 ± 0.61 %ID/g at 6 and 24 h p.i, respectively. Toledo tumor-bearing BALB/c nude mice lungs and intestine radioactivity levels were 12.90 ± 4.10 and 3.02 ± 0.49 %ID/g, and 5.56 ± 1.17 and 1.47 ± 0.31 %ID/g at 6 and 24 h p.i, respectively.

MM1S and Toledo tumor-bearing BALB/c nude mice reveled relevant ^{99m}Tc-HYNIC-Bevacizumab tumor uptake and retention. Tumor uptake in MM1S tumor-bearing BALB/c nude mice were 2.64 ± 0.22% ID/g and 2.91 ± 0.50 % ID/g at 6 and 24 h p.i, respectively. Tumor uptake in Toledo tumor-bearing BALB/c nude mice were 6.81 ± 0.87% ID/g and 8.76 ± 3.70 % ID/g at 6 and 24 h p.i., respectively.

MM1S tumor-bearing BALB/c nude mice showed ^{99m}Tc-HYNIC-Bevacizumab tumor-to-muscle ratios of 3.13 and 3.42 at 6 and 24 h, respectively. Toledo tumor-bearing BALB/c nude mice showed tumor-to-muscle ratios of 6.88 and 7.92 at 6 and 24 h, respectively.

Bevacizumab-Cy7 conjugation

The concentration of Cy7-Bevacizumab obtained was 2.04 mg/mL, with a Cy7/Bevacizumab ratio of 2.6.

Molecular imaging

SPECT/CT imaging: ^{99m}Tc-HYNIC-Bevacizumab SPECT/CT images showed an irregular liver uptake in healthy and MM1S and Toledo tumor-bearing mice at 6 and 24 h p.i. (Figures 5 and 6). Beside liver uptake there were significant heart, spleen, kidney, bladder, lungs and intestine uptake at 6 h p.i. similar to our biodistribution findings (Figure 5.A and 6.A). Discrete tumor uptake was also evident in the back of the mice where MM cells were inoculated and in the lymph

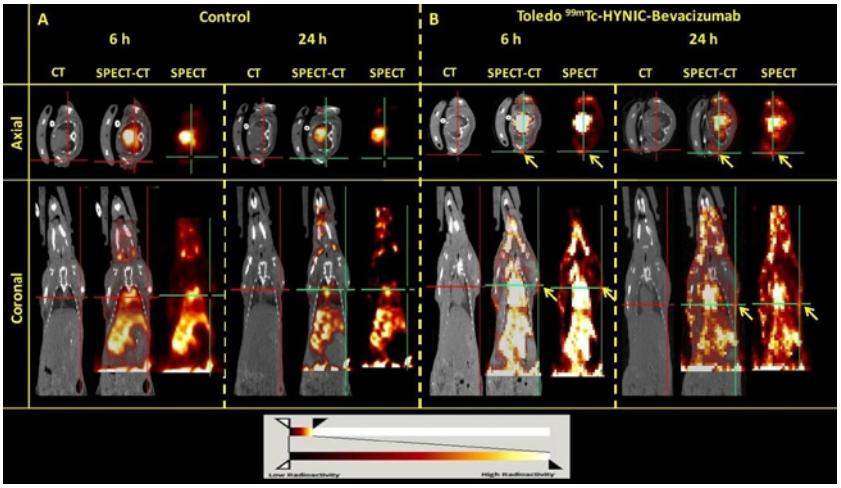

Figure 6: SPECT/CT axial and coronal images at 6 and 24 h post-injection of ^{99m}Tc-HYNIC-Bevacizumab on healthy (A) and Toledo tumor-bearing BALB/c nude mice (B). BALB/c nude mice SPECT/CT image shows non homogeneous heart, spleen, liver, kidney, bladder and gastrointestinal uptake and Toledo tumor-bearing BALB/c nude mice SPECT/CT shows a remarkable uptake of the radiolabeled Bevacizumab in the lymph nodes (tumor uptake, yellow arrows).

nodes in the NHL model (Figure 5.B and 6.B). Tumor visualization was possible at 6 and 24 h, respectively.

Fluorescent imaging: Real-time imaging studies using Cy7-Bevacizumab corroborated the previously quantified biodistribution results (Figure 7). Two MM1S and Toledo tumor-bearing mice were injected intravenously with 100µg of Cy7-Bevacizumab and were followed and quantified at 2, 24, 48, 72 and 96 h. Healthy BALB/c nude mice were used as control. Images showed clear liver and tumor (site of MM1S inoculation and lymph nodes) uptake of Cy7-Bevacizumab fluorescence (Figure 7). Also, it was possible to observe increased retention and fluorescence of Cy7-Bevacizumab in the tumor in both models up to 96h p.i. *Ex-vivo* analysis at 96h p.i. in Toledo tumor-bearing mice reveled a significant retention of Cy7-Bevacizumab in the lymph nodes corroborates the biodistribution results and SPECT/CT images.

Discussion

Tumor VEGF *in vivo* real time imaging expression has the potential to open the path to novel antiangiogenic diagnostic and therapeutic options. In this way, we evaluate *in vivo* VEGF expression in liquid hematological tumors such as MM and LNH through ^{99m}Tc via HYNIC as bifunctional chelating agent and Cy7-labeled Bevacizumab. We designed and evaluated ^{99m}Tc-HYNIC and Cy7 Bevacizumab as a specific LNH and MM imaging agent, taking into account ^{99m}Tc widespread availability and our experience labeling antibodies with ^{99m}Tc-HYNIC [68-70,90-94].

MM1S multiple myeloma and Toledo non-Hodgkin's lymphoma cell lines have been reported to express VEGF [98-101], so these cell lines were used for *in vitro* characterization of FITC-labeled Bevacizumab to confirm its VEGF binding affinity and specificity. Flow cytometric analysis using FITC-Bevacizumab showed differences in the level of expression between membrane-bound and intracellular VEGF, clearly demonstrating that in the cell lines tested, this factor is mainly expressed intracellularly. These results allowed us to perform *in vivo* studies and for this purpose we developed MM and NHL tumor models based on the induction of MM1S and Toledo cell lines in female BALB/c nude mice.

Biodistribution studies with ^{99m}Tc-HYNIC-Bevacizumab in healthy and tumor-bearing BALB/c mice show, that blood clearance is slow and that a longer-lived radioisotope would be an interesting option to work with. Although until now, we are not aware that there were any prior studies that combined MM, NHL and ^{99m}Tc-HYNIC-Bevacizumab. We must remember that these are liquid tumors, not solid ones, and SPECT-CT imaging of a tumor-bearing Balb/C Nude mice does not exactly reflect what happens in these diseases and their distributions, but they are a standardized model to work with. From our results we can see that supradiafragmatic, head and axial and appendicular skeleton can be evaluated without much interference. Abdomen, due to radiotracer elimination has its limitations to image interpretation that could be enhanced with hybrid SPECT/CT imaging. These results were also seen in the biodistributions studies in both tumor models. Tumor-to-muscle ratio increased with time and are similar to the ones reported with other ^{99m}Tc-radiolabeled antibodies [69,91,95,96].

We also performed *in vivo* VEGF expression of these liquid tumors using Cy7-Bevacizumab. Labeling and images allowed us to visualize these tumors with greater spatial resolution than SPECT.

We have already reported ^{99m}Tc-labeled Bevacizumab in solid tumors [68-70] and also Cy7-Bevacizumab in LNH [97], and we would be very interested in performing a hybrid (double-labeled) agent, and thus combine the strengths of both modalities to apply the concepts of Guided intraOperative Scintigraphic Tumor Targeting and Guided Hybrid Intra Operative Specific Targeting for the assessment of VEGF expression levels associated with NHL and MM [102-110].

We believe that these fluorescent and radiolabeled antibodies have great diagnostic and therapeutic potential that has yet to be explored. These are the first steps towards it implementation, our results are promising, the work is not finished but show that it is feasible although possible limitations due to suboptimal ^{99m}Tc properties.

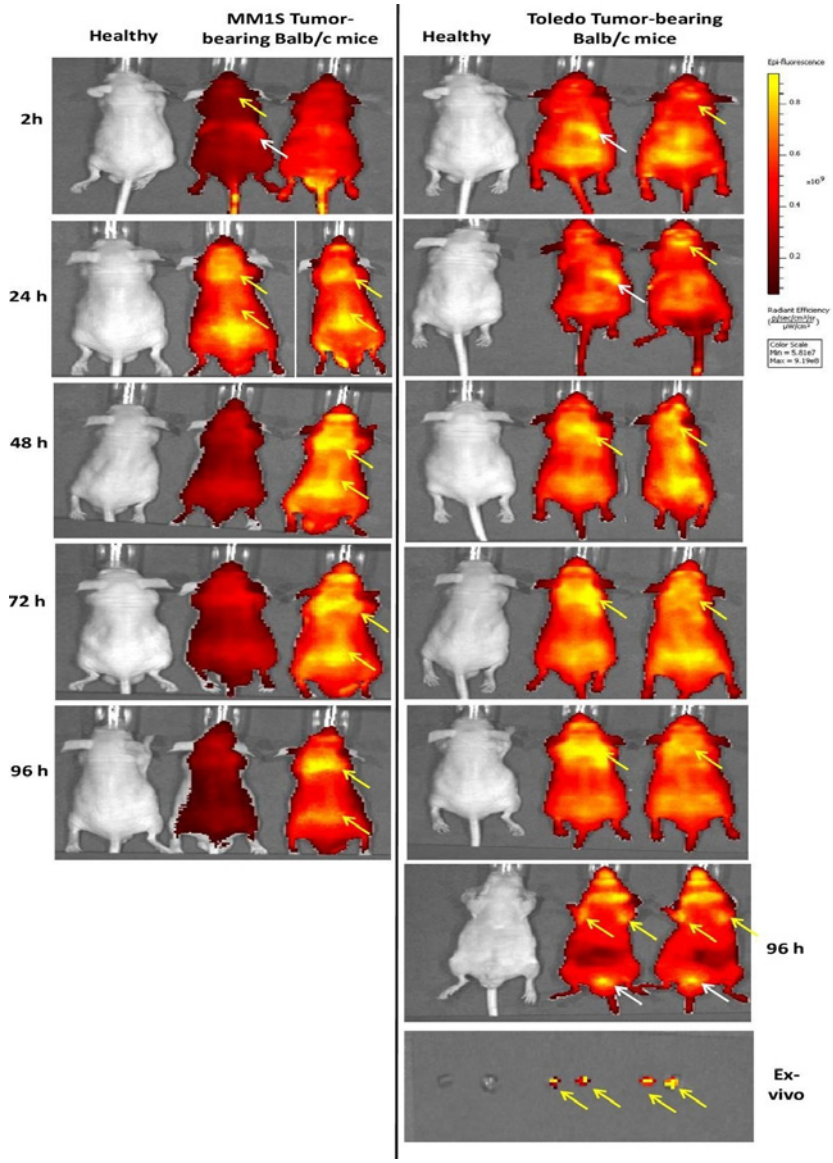

Figure 7: Fluorescence imaging. Healthy BALB/c nude mice (control) and MM1S and Toledo tumor-bearing BALB/c nude mice fluorescence imaging showed clear liver (white arrows) and tumor uptake (site of MM1S line cells inoculation and lymph nodes, yellow arrows) of Cy7-Bevacizumab fluorescence. Also, it was possible to observe increased retention and fluorescence of Cy7-Bevacizumab in tumor in both models up to 96h p.i. *Ex-vivo* fluorescence imaging of lymph node at 96h p.i. in Toledo tumor-bearing mice reveled a significant retention of Cy7-Bevacizumab corroborates the biodistribution results and SPECT/CT images.

Conclusion

MM and LNH is a deadly, frequent disease, and molecular imaging is used to monitor their progression.

The development of specific targeting probes such as Bevacizumab that targets VEGF opens the path to new ways to understand this disease, and provide novel diagnostic and therapeutic options. We successfully developed ^{99m}Tc and Cy7-labeled anti-VEGF mAb (Bevacizumab) to be used to target VEGF expression *in vivo* in MM and LNH. Our encouraging results, although working with ^{99m}Tc, highlight the importance of radioinmuno oncology as a potential tool to fight these diseases. Optical imaging of these tracers would enhance tumor sampling and guide surgical removal.

Declaration

Ethics approval and consent to participate: All the procedures were approved by the Ethical Committee for Animal Research of the Faculdade de Medicina da Universidade de São Paulo (procedure approval number 279/12), Brazil, and the Uruguayan Animal Experimentation Ethics Committee (procedure approval number 240011-002308-14), Uruguay.

Funding: This work was supported by Agencia Nacional de Innovación e Investigación (Uruguay) [POS_NAC_2015_1_109490] and Comisión Sectorial de Investigación Científica-Universidad de la República (Uruguay) [240600-000148-18].

Acknowledgments: The authors are grateful to Roche® for

providing Bevacizumab, Pro.In.Bio (Uruguay), PEDECIBA Química (Uruguay), Agencia Nacional de Innovación e Investigación (Uruguay) and Comisión Sectorial de Investigación Científica - Universidad de la República (Uruguay).

References

1. Yang J, Li W, He X, Zhang G, Yue L, Chai Y. VEGF overexpression is a valuable prognostic factor for non-Hodgkin's lymphoma evidence from a systemic meta-analysis. Dis Markers. 2015; 786790.
2. Hanahan D, Weinberg RA. Hallmarks of cancer: the next generation. Cell. 2011; 144: 646-674.
3. Ribatti D, Nico B, Ranieri G, Specchia G, Vacca A. The role of angiogenesis in human non-Hodgkin lymphomas. Neoplasia. 2013; 15: 231-238.
4. Jiang L, Li N. B-cell non-Hodgkin lymphoma: importance of angiogenesis and antiangiogenic therapy. Angiogenesis. 2020; 23: 515-529.
5. Kumar S, Witzig T, Timm M, Haug J, Wellik L, Fonseca R, et al. Expression of VEGF and its receptors by myeloma cells. Leukemia. 2003; 17: 2025-2031.
6. Ribatti D, Vacca A. New Insights in Anti-Angiogenesis in Multiple Myeloma. Int J Mol Sci. 2018; 19: 2031.
7. Ria R, Melaccio A, Racanelli V, Vacca A. Anti-VEGF Drugs in the Treatment of Multiple Myeloma Patients. J Clin Med. 2020; 9: 1765.
8. Palta A, Kaur M, Tahlan A, Dimri K. Evaluation of Angiogenesis in Multiple Myeloma by VEGF Immunoexpression and Micro vessel Density. J Lab Physicians. 2020; 12: 38-43.
9. Podar K, Tai YT, Davies FE, Lentzsch S, Sattler M, Hideshima T, et al. Vascular endothelial growth factor triggers signaling cascades mediating multiple myeloma cell growth and migration. Blood. 2001; 98: 428-435.
10. Koch S, Claesson-Welsh L. Signal transduction by vascular endothelial growth factor receptors. Cold Spring Harb Perspect Med. 2012; 2: a006502.
11. Roberts WG, Palade GE. Increased microvascular permeability and endothelial fenestration induced by vascular endothelial growth factor. J Cell Sci. 1995; 108: 2369-2379.
12. Brogi E, Wu T, Namiki A, Isner JM. Indirect angiogenic cytokines upregulate VEGF and bFGF gene expression in vascular smooth muscle cells, whereas hypoxia upregulates VEGF expression only. Circulation. 1994; 90: 649-652.
13. Kikuchi K, Kusama K, Sano M, Nakanishi Y, Ishige T, Ohni S, et al. Vascular endothelial growth factor and dendritic cells in human squamous cell carcinoma of the oral cavity. Anticancer Res. 2006; 26: 1833-1848.
14. Zhu L, Niu G, Fang X, Chen X. Preclinical molecular imaging of tumor angiogenesis. Q J Nucl Med Mol Imaging. 2010; 54: 291-308.
15. Kiselyov A, Balakin KV, Tkachenko SE. VEGF/VEGFR signaling as a target for inhibiting angiogenesis. Expert Opin Investig Drugs. 2007; 16, 83-107.
16. Tortora G, Melisi D, Ciardiello F. Angiogenesis: A target for cancer therapy. Curr Pharm Des. 2004; 10: 11-26.
17. Kubo K, Shimizu T, Ohyama S, Murooka H, Iwai A, Nakamura K, et al. Novel Potent Orally Active Selective VEGFR-2 Tyrosine Kinase Inhibitors: Synthesis, Structure-Activity Relationships, and Antitumor Activities of N-Phenyl-N0-{4-(4-quinolyloxy)phenyl} ureas. J Med Chem. 2005; 48: 1359-1366.
18. Wedge SR, Kendrew J, Hennequin LF, Valentine PJ, Barry ST, Brave SR, et al. AZD2171: A highly potent, orally bioavailable, vascular endothelial growth factor receptor-2 tyrosine kinase inhibitor for the treatment of cancer. Cancer Res. 2005; 65: 4389-4400.
19. Shrivastava A, von Wronski MA, Sato AK, Dransfield DT, Sexton D, Bogdan N, et al. A distinct strategy to generate high-affinity peptide binders to receptor tyrosine kinases. Protein Eng Des Sel. 2005; 18: 417-424.
20. Roskoski R. Sunitinib: A VEGF and PDGF receptor protein kinase and angiogenesis inhibitor. BioChem. Biophys. Res. Commun. 2007; 356: 323-328.
21. Rüegg C, Hasmim M, Lejeune FJ, Alghisi GC. Antiangiogenic peptides and proteins: From experimental tools to clinical drugs. Biochim Biophys Acta. 2006; 1765: 155-177.
22. Le Tourneau C, Raymond E, Faivre S. Sunitinib: A novel tyrosine kinase inhibitor. A brief review of its therapeutic potential in the treatment of renal carcinoma and gastrointestinal stromal tumors (GIST). Ther Clin Risk Manag. 2007; 3: 341-348.
23. Murukesh N, Dive C, Jayson GC. Biomarkers of angiogenesis and their role in the development of VEGF inhibitors. Br J Cancer. 2010; 102: 8-18.
24. Backer MV, Backer JM. Imaging key biomarkers of tumor angiogenesis. Theranostics. 2012; 2: 502-515.
25. Muñoz C, Adasen F, Alzate-Morales J, Vergara A, Kniess T, Caballero J. Study of differences in the VEGFR2 inhibitory activities between semaxanib and SU5205 using 3D-QSAR, docking, and molecular dynamics simulations. J Mol Graph Model. 2012; 32: 39-48.
26. Feliz LR, Tsimberidou AM. Anti-vascular endothelial growth factor therapy in the era of personalized medicine. Cancer Chemother Pharmacol. 2013; 72: 1-12.
27. Zhao Y, Adjei AA. Targeting Angiogenesis in Cancer Therapy: Moving Beyond Vascular Endothelial Growth Factor. Oncologist. 2015; 20: 660-673.
28. Bueno MJ, Mouron S, Quintela-Fandino M. Personalizing and targeting antiangiogenic resistance: A complex and multifactorial approach. Br J Cancer. 2017; 116: 1119-1125.
29. Simon T, Gagliano T, Giamas G. Direct Effects of Anti-Angiogenic Therapies on Tumor Cells: VEGF Signaling. Trends Mol Med. 2017; 23: 282-292.
30. Zirlik K, Duyster J. Anti-Angiogenics: Current Situation and Future Perspectives. Oncol Res Treat. 2018; 41: 166-171.
31. Garcia-Quintanilla L, Luaces-Rodríguez A, Gil-Martínez M, Mondelo-García C, Maroñas O, Mangas-Sanjuan V, et al. Pharmacokinetics of Intravitreal Anti-VEGF Drugs in Age-Related Macular Degeneration. Pharmaceutics. 2019; 11: 365.
32. Ferrara N, Hillan KJ, Gerber HP, Novotny W. Discovery and development of bevacizumab, an anti-VEGF antibody for treating cancer. Nat Rev Drug Discov. 2004; 3: 391-400.
33. Haubner R, Beer AJ, Wang H, Chen X. Positron emission tomography tracers for imaging angiogenesis. Eur J Nucl Med Mol Imaging. 2010: 37: S86-S103.
34. Kniess T. Radiolabeled small molecule inhibitors of VEGFR-Recent advances. Curr Pharm Des. 2012; 18: 2867-2874.
35. Bernard-Gauthier V, Bailey JJ, Berke S, Schirrmacher R. Recent Advances in the Development and Application of Radiolabeled Kinase Inhibitors for PET Imaging. Molecules. 2015; 20: 22000-22027.
36. Yoshimoto M, Kurihara H, Fujii H. Theragnostic Imaging Using Radiolabeled Antibodies and Tyrosine Kinase Inhibitors. Sci. World J. 2015; 842101.
37. Presta LG, Chen H, O'Connor SJ, Chisholm V, Meng YG, Krummen L, et al. Humanization of an anti- vascular endothelial growth factor monoclonal antibody for the therapy of solid tumors and other disorders. Cancer Res. 1997; 57: 4593-4599.
38. Hurwitz H, Fehrenbacher L, Novotny W, Cartwright T, Hainsworth J, Heim W, et al. Bevacizumab plus irinotecan, fluorouracil, and leucovorin for metastatic colorectal cancer. N Engl J Med. 2004; 350: 2335-2342.
39. Jayson GC, Zweit J, Jackson A, Mulatero C, Julyan P, Ranson M, et al. Molecular imaging and biological evaluation of HuMV833 anti-VEGF antibody: Implications for trial design of antiangiogenic antibodies. J Natl. Cancer Inst. 2002; 94: 1484-1493.
40. Collingridge DR, Carroll VA, Glaser M, Aboagye EO, Osman S, Hutchinson OC, et al. The Development of [124I] Iodinated-VG76e: A Novel Tracer for Imaging Vascular Endothelial Growth Factor *in Vivo* Using Positron Emission Tomography. Cancer Res. 2002; 62: 5912-5919.
41. Bouziotis P, Psimadas D, Fani M, Gourni E, Loudos G, Xanthopoulos S,

et al. Radiolabeled biomolecules for early cancer detection and therapy via angiogenesis targeting. Nucl Instrum Methods Phys Res A. 2006; 569: 492-496.

42. Fani M, Bouziotis P, Harris AL, Psimadas D, Gourni E, Loudos G, et al. 177Lu-labeled-VG76e monoclonal antibody in tumor angiogenesis: A comparative study using DOTA and DTPA chelating systems. Radiochim Acta. 2007; 95: 351-357.

43. Willmann JK, Paulmurugan R, Chen K, Gheysens O, Rodriguez-Porcel M, Lutz AM, et al. US imaging of tumor angiogenesis with microbubbles targeted to vascular endothelial growth factor receptor type 2 in mice. Radiology. 2008; 246: 508-518.

44. Willmann JK, Cheng Z, Davis C, Lutz AM, Schipper ML, Nielsen CH, et al. Targeted microbubbles for imaging tumor angiogenesis: Assessment of whole-body biodistribution with dynamic micro-PET in mice. Radiology. 2008; 249: 212-219.

45. Lee CM, Kim EM, Cheong SJ, Kim DW, Lim ST, Sohn MH, et al. Targeted molecular imaging of VEGF receptors overexpressed in ischemic microvasculature using chitosan-DC101 conjugates. J Biomed Mater Res A. 2010; 92: 1510-1517.

46. Desar IME, Stillebroer AB, Oosterwijk E, Leenders WPJ, van Herpen CML, van der Graaf WTA, et al. 111In-Bevacizumab Imaging of Renal Cell Cancer and Evaluation of Neoadjuvant Treatment with the Vascular Endothelial Growth Factor Receptor Inhibitor Sorafenib. J Nucl Med. 2010; 51: 1707-1715.

47. Chang AJ, Sohn R, Lu ZH, Arbeit JM, Lapi SE. Detection of Rapalog-Mediated Therapeutic Response in Renal Cancer Xenografts Using 64Cu-bevacizumab ImmunoPET. PLoS ONE. 2013; 8: e58949.

48. Nagengast WB, de Vries EGE, Hospers GA, Mulder NH, de Jong JR, Hollema H, et al. *In Vivo* VEGF Imaging with Radiolabeled Bevacizumab in a Human Ovarian Tumor Xenograft. J Nucl Med. 2007; 48: 1313-1319.

49. Scheer MG, Stollman TH, Boerman OC, Verrijp K, Sweep FCGJ, Leenders WPJ, et al. Imaging liver metastases of colorectal cancer patients with radiolabelled bevacizumab: Lack of correlation with VEGF-A expression. Eur J Cancer. 2008; 44: 1835-1840.

50. Nagengast WB, Lub-de Hooge MN, van Straten EME, Kruijff S, Brouwers AH, den Dunnen WFA, et al. VEGF-SPECT with 111In-bevacizumab in stage III/IV melanoma patients. Eur J Cancer. 2011; 47: 1595-1602.

51. Stollman TH, Scheer MGW, Leenders WPJ, Verrijp KCN, Soede AC, Oyen WJG, et al. Specific imaging of VEGF-A expression with radiolabeled anti-VEGF monoclonal antibody. Int J Cancer. 2008; 122: 2310-2314.

52. Stollman TH, Scheer MG, Franssen GM, Verrijp KN, Oyen WJG, Ruers TJM, et al. Tumor accumulation of radiolabeled bevacizumab due to targeting of cell- and matrix-associated VEGF-A isoforms. Cancer Biother Radiopharm. 2009; 24: 195-200.

53. Hosseinimehr SJ, Orlova A, Tolmachev V. Preparation and *in vitro* evaluation of 111In-CHX-A"-DTPA-labeled anti-VEGF monoclonal antibody bevacizumab. Hum Antibodies. 2010; 19: 107-111.

54. Nayak TK, Garmestani K, Baidoo KE, Milenic DE, Brechbiel MW. PET imaging of tumor angiogenesis in mice with VEGF-A targeted 86Y-CHX-A"-DTPA-bevacizumab. Int J Cancer. 2011; 128: 920-926.

55. Van Dongen GAMS, Poot AJ, Vugt DJ. PET imaging with radiolabeled antibodies and tyrosine kinase inhibitors: Immuno-PET and TKI-PET. Tumor Biol. 2012; 33: 607-615.

56. Kameswaran M, Pandey U, Gamre N, Vimalnath KV, Sarma HD, Dash A. Evaluation of (177)Lu-CHX-A"-DTPABevacizumab as a radioimmunotherapy agent targeting VEGF expressing cancers. Appl Radiat Isot. 2016; 114: 196-201.

57. Patel N, Able S, Allen D, Fokas E, Cornelissen B, Gleeson FV, et al. Monitoring response to antiangiogenic mTOR inhibitor therapy in vivo using 111In-bevacizumab. EJNMMI Res. 2017; 7: 49.

58. Yudistiro R, Hanaoka H, Katsumata N, Yamaguchi A, Tsushima Y. Bevacizumab Radioimmunotherapy (RIT) with Accelerated Blood Clearance Using the Avidin Chase. Mol Pharm. 2018; 15: 2165-2173.

59. Nagengast WB, de Korte MA, Munnink THO, Timmer-Bosscha H, den Dunnen WF, Hollema H, et al. ^{89}Zr-Bevacizumab PET of Early Antiangiogenic Tumor Response to Treatment with HSP90 Inhibitor NVP-AUY922. J Nucl Med. 2010; 51: 761-767.

60. Van der Bilt AR, Terwisscha van Scheltinga AG, Timmer-Bosscha H, Schröder CP, Pot L, Kosterink JGW, et al. Measurement of tumor VEGF-A levels with ^{89}Zr-bevacizumab PET as an early biomarker for the antiangiogenic effect of everolimus treatment in an ovarian cancer xenograft model. Clin Cancer Res. 2012; 18: 6306-6314.

61. Van Asselt SJ, Oosting SF, Brouwers AH, Bongaerts AHH, de Jong JR, Lub-de Hooge MN, et al. Everolimus Reduces ^{89}Zr-Bevacizumab Tumor Uptake in Patients with Neuroendocrine Tumors. J Nucl Med. 2014; 55: 1087-1092.

62. Van Es SC, Brouwers AH, Mahesh SVK, Leliveld-Kors AM, de Jong IJ, Lub-de Hooge MN, et al. ^{89}Zr-Bevacizumab PET: Potential Early Indicator of Everolimus Efficacy in Patients with Metastatic Renal Cell Carcinoma. J Nucl Med. 2017; 58: 905-910.

63. Gaykema SBM, Brouwers AH, Lub-de Hooge MN, Timmer-Bosscha H, Pot L, van Dam GM, et al. ^{89}Zr-Bevacizumab PET Imaging in Primary Breast Cancer. J Nucl Med. 2013; 54: 1014-1018.

64. Bahce I, Huisman MC, Verwer EE, Ooijevaar R, Boutkourt F, Vugts DJ, et al. Pilot study of ^{89}Zr-bevacizumab positron emission tomography in patients with advanced non-small cell lung cancer. EJNMMI Res. 2014; 4: 35.

65. Oosting S, Brouwers AH, Van Es SC, Nagengast WB, Munnink THO, Hooge MNL, et al. ^{89}Zr-bevacizumab PET imaging in metastatic renal cell carcinoma patients before and during antiangiogenic treatment. J Clin Oncol. 2012; 30: 10581.

66. Oosting SF, Brouwers AH, Van Es SC, Nagengast WB, Munnink THO, Hooge MNL, et al. ^{89}Zr-bevacizumab PET visualizes heterogeneous tracer accumulation in tumour lesions of renal cell carcinoma patients and differential effects of antiangiogenic treatment. J Nucl Med. 2015; 56: 63-69.

67. Oosting FS, van Asselt SJ, Brouwers AH, Bongaerts AHH, Steinberg, JDJ, de Jong, JR, et al. ^{89}Zr-Bevacizumab PET Visualizes Disease Manifestations in Patients with von Hippel-Lindau Disease. J Nucl Med. 2016; 57: 1244-1250.

68. Camacho X, García MF, Calzada V, Fernández M, Porcal W, Alonso O, et al. Synthesis and evaluation of ^{99m}Tc chelate-conjugated bevacizumab. Curr Radiopharm. 2013; 6: 12-19.

69. Camacho X, García MF, Calzada V, Fernández M, Chabalgoity JA, Moreno M, et al. ^{99m}Tc(CO)3-Radiolabeled Bevacizumab: *In vitro* and *in vivo* Evaluation in a Melanoma Model. Oncology. 2013; 84: 200-209.

70. Camacho X, García MF, Calzada V, Fernández M, Alonso O, Gambini JP, et al. ^{99m}Tc-Labeled Bevacizumab via HYNIC for Imaging of Melanoma. J Anal Oncol. 2014; 3: 53-64.

71. Kameswaran M, Pandey U, Sarma HD, Samuel G. Preparation of ^{99m}Tc carbonyl DTPA-bevacizumab and its bioevaluation in a melanoma model. Ann Nucl Med. 2014; 28: 911-916.

72. Cohen R, Stammes MA, de Roos IH, Stigter-van Walsum M, Visser GW, van Dongen GA. Inert coupling of IRDye800CW to monoclonal antibodies for clinical optical imaging of tumor targets. EJNMMI Res. 2011; 1: 31.

73. Cohen R, Vugts DJ, Stigter-van Walsum M, Visser GW, van Dongen GA. Inert coupling of IRDye800CW and zirconium-89 to monoclonal antibodies for single- or dual-mode fluorescence and PET imaging. Nat Protoc. 2013; 8: 1010-1018.

74. Jansen MH, Lagerweij T, Sewing AC, Vugts DJ, van Vuurden DG, Molthoff CFM, et al. Bevacizumab Targeting Diffuse Intrinsic Pontine Glioma: Results of 89Zr-Bevacizumab PET Imaging in Brain Tumor Models. Mol Cancer Ther. 2016; 15: 2166-2174.

75. Jansen MH, Veldhuijzen van Zanten SEM, van Vuurden DG, Huisman MC, Vugts DJ, Hoekstra OS, et al. Molecular Drug Imaging: 89Zr-Bevacizumab PET in Children with Diffuse Intrinsic Pontine Glioma. J Nucl Med. 2017; 58: 711-716.

76. Veldhuijzen van Zanten SEM, Sewing ACP, van Lingen A, Hoekstra OS, Wesseling P, Meel MH, et al. Multiregional Tumor Drug-Uptake Imaging by PET and Microvascular Morphology in End-Stage Diffuse Intrinsic Pontine Glioma. J Nucl Med. 2018; 59: 612-615.

77. Ashrafi SA, Hosseinimehr SJ, Varmira K, Abedi SM. Radioimmunotherapy with 131I-bevacizumab as a specific molecule for cells with overexpression of the vascular endothelial growth factor. Cancer Biother Radiopharm. 2012; 27: 420-425.

78. Kameswaran M, Sarma HD, Dash A. Preclinical evaluation of 131I-Bevacizumab-A prospective agent for radioimmunotherapy in VEGF expressing cancers. Appl Radiat Isot. 2017; 123: 109-113.

79. Christoforidis JB, Carlton MM, Knopp MV, Hinkle GH. PET/CT imaging of I-124-radiolabeled bevacizumab and ranibizumab after intravitreal injection in a rabbit model. Invest. Ophthalmol. Vis Sci. 2011; 52: 5899-5903.

80. Christoforidis JB, Carlton MM, Wang J, Jiang A, Pratt C, Abdel-Rasoul M, et al. Anatomic and pharmacokinetic properties of intravitreal bevacizumab and ranibizumab after vitrectomy and lensectomy. Retina. 2013; 33: 946-952.

81. Christoforidis JB, Briley K, Binzel K, Bhatia P, Wei L, Kumar K, et al. Systemic Biodistribution and Intravitreal Pharmacokinetic Properties of Bevacizumab, Ranibizumab, and Aflibercept in a Nonhuman Primate Model. Invest. Ophthalmol. Vis Sci. 2017; 58: 5636-5645.

82. Paudyal B, Paudyal P, Oriuchi N, Hanaoka H, Tominaga H, Endo K. Positron emission tomography imaging and biodistribution of vascular endothelial growth factor with 64Cu-labeled bevacizumab in colorectal cancer xenografts. Cancer Sci. 2011; 102: 117-121.

83. Zhang Y, Hong H, Engle JW, Yang Y, Barnhart TE, Cai W. Positron emission tomography and near-infrared fluorescence imaging of vascular endothelial growth factor with dual-labeled bevacizumab. Am J Nucl Med Mol. Imaging. 2012; 2: 1-13.

84. Luo H, England CG, Graves SA, Sun H, Liu G, Nickles RJ, et al. PET Imaging of VEGFR-2 Expression in Lung Cancer with 64Cu-Labeled Ramucirumab. J Nucl Med. 2016; 57: 285-290.

85. Li M, Jiang D, Barnhart TE, Cao T, Engle JW, Chen W, et al. Immuno-PET imaging of VEGFR-2 expression in prostate cancer with ^{89}Zr-labeled ramucirumab. Am J Cancer Res. 2019; 9: 2037-2046.

86. Janousek J, Barta P, Novy Z, Zilkova K, Trejtnar F. Antiangiogenic Human Monoclonal Antibody Ramucirumab Radiolabelling: *In Vitro* Evaluation on VEGFR2-positive Cell Lines. Anticancer Res. 2019; 39: 735-744.

87. Nagengast WB, Lub-de Hooge MN, Oosting SF, den Dunnen WFA, Warnders FJ, Brouwers AH, et al. VEGF-PET Imaging Is a Noninvasive Biomarker Showing Differential Changes in the Tumor during Sunitinib Treatment. Cancer Res. 2011; 71: 143-154.

88. Te Velde EA, Veerman T, Subramaniam V, Ruers T. The use of fluorescent dyes and probes in surgical oncology. Eur J Surg Oncol. 2010; 36: 6-15.

89. Frangioni JV. *In vivo* near-infrared fluorescence imaging. Curr Opin Chem Biol. 2003; 7: 626-634.

90. Camacho X, Machado CL, García MF, Gambini JP, Banchero A, Fernández M, et al. Technetium-^{99m}- or Cy7-Labeled Rituximab as an Imaging Agent for Non-Hodgkin Lymphoma. Oncology. 2017; 92: 229-242.

91. Camacho X, Machado CL, García MF, Fernández M, Oddone N, Benech J, et al. Tocilizumab Labeling with ^{99m}Technetium via HYNIC as a Molecular Diagnostic Agent for Multiple Myeloma. Anticancer Agents Med Chem. 2017; 17: 1267-1277.

92. Camacho X, Perroni C, Machado CL, Carneiro CG, Junqueira MS, Faria D, et al. ^{99m}Technetium- or Cy7-Labeled Fab(Tocilizumab) as Potential Multiple Myeloma Imaging Agents. Anticancer Agents Med Chem. 2021; 21: 1883-1893.

93. Perroni C, Camacho X, García MF, Fernández M, Cerecetto H, Gambini JP, et al. ^{99m}Tc-HYNIC-Fab (Bevacizumab): Potencial agente de imagen para diagnóstico de Linfoma No Hodgkin. Salud Militar. 2017; 36: 14-24.

94. Calzada V, García MF, Alonso-Martínez LM, Camacho X, Goicochea E, Fernández M, et al. Fab(nimotuzumab)-HYNIC-^{99m}Tc: Antibody Fragmentation for Molecular Imaging Agents. Anticancer Agents Med Chem. 2016; 16: 1184-1189.

95. Camacho X, Machado CL, García MF, Gambini JP, Banchero A, Fernández M, et al. Technetium-^{99m}- or Cy7-Labeled Rituximab as an Imaging Agent for Non-Hodgkin Lymphoma. Oncology. 2017; 92: 229-242.

96. Garcia MF, Camacho X, Calzada V, Fernández M, Porcal W, Alonso O, et al. Synthesis of ^{99m}Tc-nimotuzumab with tricarbonyl ion: *in vitro* and *in vivo* studies. Curr Radiopharm. 2012; 5: 59-64.

97. Camacho X, Perroni C, de Souza Junqueira M, Fernández M, Bustos S, Buchpiguel C, et al. Near-Infrared Fluorescence *In-Vivo* Imaging of Non-Hodgkin Lymphoma Using Cy7-Bevacizumab. Blood. 2017; 130: 5202.

98. Kumar S, Witzig TE, Timm M, Haug J, Wellik L, Fonseca R, et al. Expression of VEGF and its receptors by myeloma cells. Leukemia. 2003; 17: 2025-2031.

99. Gupta D, Treon SP, Shima Y, Hideshima T, Podar K, Tai YT, et al. Adherence of multiple myeloma cells to bone marrow stromal cells upregulates vascular endothelial growth factor secretion: therapeutic applications. Leukemia. 2001; 15: 1950-1961.

100. Wang J, Chen J, Qiu D, Zeng Z. Regulatory role of DEPTOR-mediated cellular autophagy and mitochondrial reactive oxygen species in angiogenesis in multiple myeloma. Int J Mol Med. 2021; 47: 643-658.

101. Mori F, Ishida T, Ito A, Sato F, Masaki A, Takino H, et al. Potent antitumor effects of bevacizumab in a microenvironment-dependent human lymphoma mouse model. Blood Cancer J. 2012; 2: e67.

102. Rijpkema M, Bos DL, Cornelissen AS, Franssen GM, Goldenberg DM, Oyen WJ, et al. Optimization of Dual-Labeled Antibodies for Targeted Intraoperative Imaging of Tumors. Mol Imaging. 2015; 14: 348-355.

103. Sampath L, Kwon S, Ke S, Wang W, Schiff R, Mawad ME, et al. Dual-labeled trastuzumab-based imaging agent for the detection of human epidermal growth factor receptor 2 overexpression in breast cancer. J Nucl Med. 2007; 48: 1501-1510.

104. Rijpkema M, Oyen WJ, Bos D, Franssen GM, Goldenberg DM, Boerman OC. SPECT- and fluorescence image-guided surgery using a dual-labeled carcinoembryonic antigen-targeting antibody. J Nucl Med. 2014; 55: 1519-1524.

105. Ogawa M, Regino CA, Seidel J, Green MV, Xi W, Williams M, et al. Dual-modality molecular imaging using antibodies labeled with activatable fluorescence and a radionuclide for specific and quantitative targeted cancer detection. Bioconjug Chem. 2009; 20: 2177-2184.

106. Aldrich MB, Wang X, Hart A, Kwon S, Sampath L, Marshall MV, et al. Assessment of free dye in solutions of dual-labeled antibody conjugates for in vivo molecular imaging. Mol Imaging Biol. 2011; 13: 32-42.

107. Dong C, Yang S, Shi J, Zhao H, Zhong L, Liu Z, et al. SPECT/NIRF Dual Modality Imaging for Detection of Intraperitoneal Colon Tumor with an Avidin/Biotin Pretargeting System Sci Rep. 2016; 6: 18905.

108. Lütje S, Rijpkema M, Franssen GM, Fracasso G, Helfrich W, Eek A, et al. Dual-Modality Image-Guided Surgery of Prostate Cancer with a Radiolabeled Fluorescent Anti-PSMA Monoclonal Antibody. J Nucl Med. 2014; 55: 995-1001.

109. Valdes Olmos RA, Vidal-Sicart S, Giammarile F, Zaknun JJ, Van Leeuwen FW, Mariani G. The GOSTT concept and hybrid mixed/virtual/augmented reality environment radioguided surgery. Q J Nuc Med Mol Imaging. 2014; 58: 207-215.

110. Gambini JP, Quinn TP. Hybrid tracers and devices for intraoperative imaging: the future for radioguided surgery? Clin Transl Imaging. 2016; 4: 343.